American Mineralogist, Volume 73, pages 161–167, 1988

X-ray photoelectron spectroscopy for the direct identification of Ti valence in $[Ba_xCs_y][(Ti,Al)^{3+}_{2x+y}Ti^{4+}_{8-2x-y}]O_{16}$ hollandites

Sverre Myhra
School of Science, Griffith University, Nathan, Queensland, Australia 4111

Timothy J. White
Materials Division, Australian Nuclear Science and Technology Organization, Lock Mail Bag No. 1, Menai, N.S.W., Australia 2234

Sue E. Kesson
Research School of Earth Sciences, Australian National University, GPO Box 4, Canberra, A.C.T., Australia 2600

John C. Riviere
Surface Analysis Section, Materials Development Division, Harwell Laboratory, Oxon OX11 0RA, United Kingdom

Abstract

A priori knowledge of the valence adopted by transition-metal elements in minerals frequently provides useful insight into their petrogenesis. Generally, one or more of the several well-established spectroscopic methods (e.g., Mössbauer, UV-visible, X-ray absorption) are used to determine the chemical state of cationic species. A more recent technique, which is now gaining increasing acceptance for such studies, is X-ray photoelectron spectroscopy (XPS). In this paper, we report the way in which XPS may be used to extract, in a semiquantitative manner, the ratio of trivalent to tetravalent Ti species in synthetic $[Ba_xCs_y][(Al,Ti^{3+})_{2x+y}Ti^{4+}_{8-2x-y}]O_{16}$ hollandites. The Ti^{3+}/Ti^{4+} ratios found by XPS are in qualitative agreement with those derived indirectly from classical electron-microprobe analysis. The quantitative discrepancies can be ascribed to the presence of rutile in minor amounts. Generalized guidelines for the use of XPS to obtain compositional and chemical information about mineral specimens are outlined.

Introduction

Although the atomic structures of many minerals have been accurately determined by X-ray or neutron diffraction, the details of their electronic structures are usually less well established. This is particularly so for minerals containing transition-metal cations that may exist in two or more oxidation states. Often the valence of the elements that constitute a mineral are inferred from its petrogenesis, but this approach may prove ambiguous if extensive alteration has occurred. Therefore, it is inherently more useful to determine directly the elemental valence, as this information will reflect the ambient oxygen fugacity during mineral formation.

In mineralogical studies, oxidation states are most commonly derived from electron-microprobe analyses (EMPA) in which oxides are summed to the desired oxygen stoichiometry. However, this approach assumes that the valence of all elements is known, and errors may occur if the chemistry is complex or the oxygen stoichiometry large (>10). To overcome these limitations, attempts have been made to develop more sophisticated EMPA techniques in which the relative intensities of the characteristic X-ray emissions for a particular element are compared. For example, O'Nions and Smith (1971) tried to use the L_{II}:L_{III} ratio of Fe to establish the content of ferrous and ferric species in wüstite, hematite, and pseudobrookite. However, they concluded that only qualitative information could be gained in this way.

Several other spectroscopic techniques are available to determine chemical speciation. Mössbauer spectroscopy has been applied to over 40 elements (Herber, 1982), though for mineralogical studies it is generally the ^{57}Fe nuclide that is exploited (e.g., Aldridge et al., 1986; Dyar and Burns, 1986). Optical absorption spectroscopy, X-ray absorption spectroscopy, and electron-paramagnetic-resonance spectroscopy are also available, but these methods are sometimes limited by the large sample volume required (e.g., Hofmeister and Rossman, 1984; Bonnin et al., 1985). Again, these methods have usually been applied to the geologically interesting ferrous-ferric species. Most recently, electron-energy-loss spectroscopy has been used to identify the valence of elements and simultaneously (in combination with electron microscopy) provide structural information from very small crystallites.

0003–004X/88/0102–0161$02.00

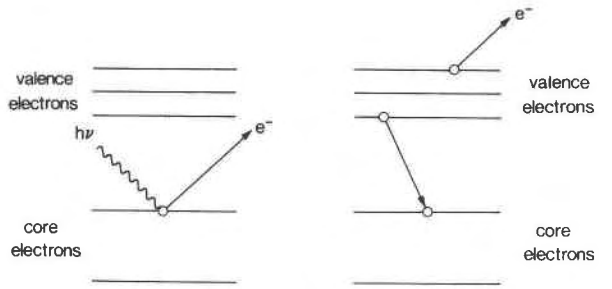

Fig. 1. (a) Schematic illustration of the process of photoelectron ejection by X-ray photons. The photoelectrons can come from either core or valence shells. (Adapted from Briggs and Seah, 1983.) (b) The ejection of Auger electrons follows the nonradiative transition of an electron to an inner-shell vacancy. (Adapted from Briggs and Seah, 1983.)

It is, however, unable to separate or quantify mixed valences of the same element (Otten et al., 1985).

XPS studies of mineral surfaces have not been reported extensively (Nefedov et al., 1972; Adams et al., 1977; Bancroft et al., 1979; Thames et al., 1981; Evans and Raftery, 1982) although application of the technique to such problems is increasing. In particular, XPS has been shown to be especially valuable for determining the mechanisms that are relevant to surface or interface reactions such as those that govern the dissolution of minerals (Schott and Berner, 1983; Myhra et al., 1984).

The present article describes how XPS may be used in mineralogical studies to ascertain semiquantitatively the proportions of mixed-valence transition-metal species. We have chosen to illustrate the utility of this technique by determining the relative proportions of trivalent and tetravalent cations in a number of well-characterized synthetic hollandite samples with the general formula $[Ba_x\text{-}Cs_y][(Al,Ti^{3+})_{2x+y}Ti^{4+}_{8-2x-y}]O_{16}$ (Kesson and White, 1986).

Principles of X-ray photoelectron spectroscopy

Briefly, XPS is based on the principle that, when a surface is irradiated with X-rays, photoelectrons will be ejected (Fig. 1a). If X-ray lines of sufficiently narrow widths are used, the photoelectrons have characteristic energies related directly to the atomic levels from which they came; XPS commonly uses either the Al$K\alpha$ (1486.6 eV) or the Mg$K\alpha$ (1253.6 eV) lines. With such low-energy excitation, the photoelectrons must originate in the outer few monolayers only if they are to escape without energy loss. The resultant energetic electrons are then collected and counted, after dispersion, by an electrostatic analyzer. A photoelectron energy spectrum then consists of a plot of counts as a function of kinetic energy. Such spectra may be used for analytical purposes or to gain insight into the chemical bonding of the elements present. The technique is fully quantitative insofar as the area under a characteristic peak can be related directly to the concentration of the corresponding atomic species in the surface layer. The sensitivity of XPS is of the order of 0.1 at.% for most elements. Chemical information can be extracted from the spectrum by detailed considerations of the position (with a typical resolution of ± 0.1 eV) and shape of peak envelopes. This information can be interpreted readily by comparison with spectra of standard compounds, recorded in the same experiment, or by consulting the voluminous and mature literature on XPS investigations of various compounds (Briggs and Seah, 1983).

XPS is generally thought of as a broad-beam technique because the normal lateral resolution is ~1 mm. However, some recent instruments are capable of "mapping" with a lateral resolution of ~100 μm. (Riviere, 1986).

Comparison with other surface analytical techniques

It is common to have XPS available in combination with at least one other surface analytical technique—usually Auger electron spectroscopy with scanning Auger microscopy (AES–SAM), and with static secondary-ion mass spectrometry (SSIMS). As summarized in Table 1, these techniques are surface specific and yield data that are essentially complementary.

The application of AES–SAM to geologic problems has been reviewed recently (Hochella et al., 1986a, 1986b). Auger electrons are generated by irradiation of the surface with monoenergetic electrons (typically 3–10 keV). As with XPS, the primary interaction is the ejection of a core electron, but in this case the characteristic event is the radiationless decay of an upper-level electron into the core vacancy and the simultaneous ejection of an Auger electron with a characteristic kinetic energy (Fig. 1b). The low (30–1000 eV) kinetic energies analyzed in AES ensure that the technique is surface specific for the same reasons as mentioned above for XPS. Again, a spectrum of characteristic peaks indicative of atomic species in the near-surface layers can be generated by electrostatic analysis, and peak heights can be related to atomic abundances. However, chemical (i.e., bonding) information cannot be as readily extracted, as in the case of XPS, since electron-excited Auger peaks are generally wider and weaker. In particular, differential Auger peak positions, which is the most common operational mode, cannot be measured with the precision of XPS peaks. The significant advantage of AES–SAM over XPS lies in its excellent lateral resolution and the ability to scan a finely focused electron beam (~20-nm diameter for the most advanced instrument) over the sample and produce elemental maps showing the lateral distribution of surface species. Such maps can be related to surface features observed by secondary-electron microscopy (see Cooper et al., 1986) for an example of Cs mapping on hollandite fracture faces).

Unlike XPS and AES–SAM, static secondary-ion mass spectrometry (SSIMS) is a destructive technique, dynamic SIMS is even more so, and at times this may limit its applicability. (There are also cases where the high current densities of AES–SAM will be destructive.) During analysis by SSIMS, an incident ion beam (usually 0.5–5 keV) is used to induce sputtering of atomic and molecular species from

TABLE 1. Comparison of surface analytical techniques

	XPS	AES–SAM	SIMS
Sampling depth (monolayers)	1–10	1–5	2 (static), 40 (dynamic)
Lateral resolution (nm)	10^6	200–1000	10^4
Sensitivity (at.%)	0.1	0.1	0.001
Nondestructive	yes	yes–no	no
Charging problems	yes	yes	yes
Elemental-mapping capability	no	yes	yes
Elemental range	$Z > 3$	$Z > 3$	all elements
Accuracy of analysis	fully quantitative	fully (AES) and semi- (SAM) quantitative	semi-quantitative
Principal application	determination of chemical speciation and composition	elemental mapping of surface species and small-area analysis	trace-element analysis

a solid surface. The incident ions are commonly Ar or oxygen but liquid metal, particularly Ga, sources are also available. The ejected species usually come from the first one or two atom layers (0.5 nm), although interlayer mixing of species may sometimes give rise to contributions from greater depths (Smart, 1985). The sputtered ions are focused onto a mass analyzer (quadrupole, electrostatic, or magnetic sector). The technique is extremely sensitive, being able to detect many species at the ppm level, and it is as a method of identifying trace elements that SSIMS is far superior to XPS and AES–SAM (Table 1). Although SSIMS is able to detect all elemental isotopes, such spectra are extremely difficult to quantify owing to the large range of ionic sensitivities and the variable sputtering rates of the same species from different matrices. However, reliable comparisons can be drawn between materials of similar composition. Because SIMS gradually erodes the surface under examination (especially in the so-called "dynamic" mode), it is often used in conjunction with the other techniques to yield depth profiled XPS or AES–SAM data.

Thus, for the purposes of the present experiment, which is the determination of Ti valence states in hollandite, XPS is the most appropriate tool. If on the other hand, the aim had been to study the spatial distribution of Cs or perhaps the occurrence of unexpected trace impurity atoms, then AES–SAM or SSIMS would have been more suitable.

EXPERIMENTAL METHODS

Specimen preparation

A detailed description of the methods used to prepare the hollandite samples has been given elsewhere (Kesson and White, 1986). In brief, titanium-2-propoxide was hydrolized and dried to produce a highly reactive form of hydrated titania. This powder was mixed with aqueous solutions of aluminum, barium, and cesium nitrates in quantities appropriate to the particular hollandite being prepared. After slurrying at pH 9 with NH_4OH, the filtered powder was calcined at 750°C for 1 h. Reactive hot pressing was then carried out using the conditions listed in Table 2. The specimens were characterized by X-ray diffraction and chemically analyzed using an electron microprobe; the derivation of structural formulae was based on these latter data. In addition to hollandite, lesser quantities of slightly reduced rutile (Ti_nO_{2n-1}) were also present and estimated to account for 15–30% of the bulk by volume. As well as the hollandite-rutile assemblages, a section of single-crystal rutile (TiO_2) was used as a reference surface in which the majority of the Ti is tetravalent.

The hollandites were fractured immediately before transfer to the spectrometer UHV chamber in order to minimize oxidation and contamination and to present a surface most likely to be representative of bulk abundances and chemical environments for all atomic species. The rutile specimen was cut perpendicular to its crystallographic c axis (±2°), and the (001) surface was polished (0.2-μm alumina powder) and etched in a bath of molten NaOH at 800°C. The specimen was then equilibrated in high-purity oxygen at 700°C, quenched to laboratory ambient, and transferred to the spectrometer air-lock in an oxygen atmosphere.

Analytical procedure

XPS data were collected using a VG ESCALAB Mark II at AERE Harwell. A survey scan was carried out for every specimen in order to confirm the presence of all expected species, to determine the extent of adventitious C contamination (i.e., weakly bound polymeric C), and to as-

TABLE 2. $[Ba_xCs_y][(Al,Ti^{3+})_{2x+y}Ti^{4+}_{8-2x-y}]O_{16}$ hollandites

Specimen no.	Structural formula	Preparation conditions
HP 462	$[Ba_{0.48}Cs_{0.70}][Ti^{3+}_{1.86}Ti^{4+}_{6.34}]O_{16}$	hot-pressed in graphite, 1250 °C, 30 MPa, 1 h
HP 465	$[Cs_{1.49}][(Al_{0.32}Ti^{3+}_{1.17})Ti^{4+}_{6.51}]O_{16}$	hot-pressed in platinum, 1250 °C, 0.5 GPa, 1 h
HP 463	$[Cs_{1.32}][Ti^{3+}_{1.32}Ti^{4+}_{6.68}]O_{16}$	hot-pressed in graphite, 1250 °C, 30 MPa, 1 h
HP 410	$[Ba_{0.65}Cs_{0.52}][(Al_{0.70}Ti^{3+}_{1.12})Ti^{4+}_{6.18}]O_{16}$	hot-pressed in graphite, 1250 °C, 30 MPa, 1 h
HP 402	$[Ba_{0.21}Cs_{0.91}][(Al_{0.66}Ti^{3+}_{0.66})Ti^{4+}_{6.66}]O_{16}$	hot-pressed in graphite, 1250 °C, 30 MPa, 1 h

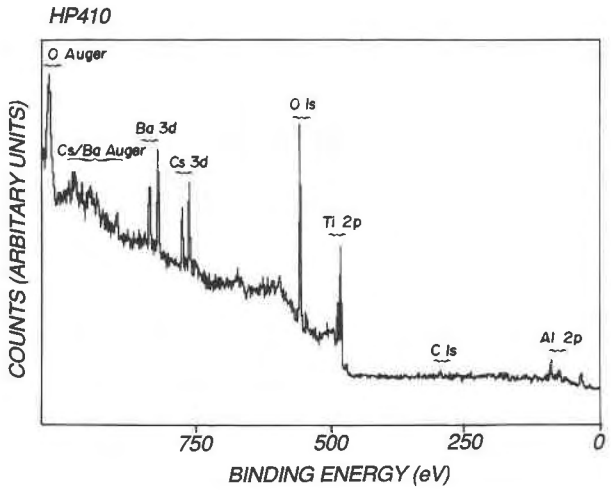

Fig. 2. Survey XPS scan of the hollandite (HP 410) surface. The major peaks are labeled in accord with standard notation. Doublets such as Ti $2p_{3/2,1/2}$, are not resolved.

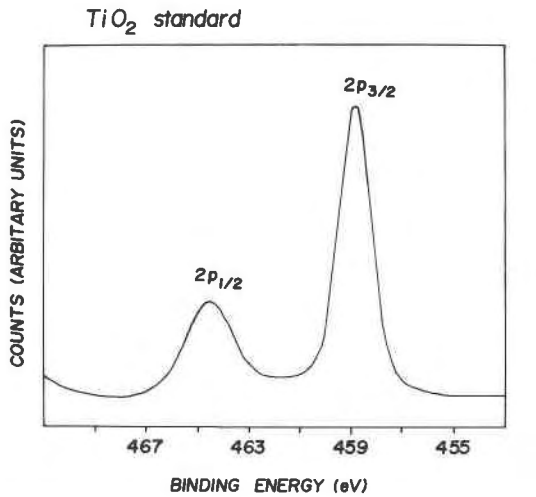

Fig. 3. Detailed XPS scan over the Ti $2p_{3/2,1/2}$ region for a single-crystal TiO_2 surface. Background has been subtracted and the envelope smoothed with a polynomial best fit in order to arrive at the standard tetravalent spectrum.

certain the severity of charging. AlK_α X-rays with a source power of 300 W were used as the incident radiation. Base vacuum was 10^{-9} torr or better; previous studies have shown that extreme UHV conditions are not required for relatively inert titanate surfaces (Myhra et al., 1983). The parameters for these survey scans were as follows: 50-eV pass energy, 1-eV increments, and 10-ms per increment. A typical survey scan (HP 402) is shown in Figure 2; the major characteristic peaks are consistent with the expected atomic species.

Detailed scans were made across all major peaks—oxygen 1*s*, Ti 2*p*, Ba 3*d*, Cs 3*d*, and Al 2*p* and 2*s*. (Adventitious C contamination was also monitored, although the fractured surfaces contained only trace amounts of this element.) The detailed scans were obtained with a pass energy of 20 eV, 0.2-eV increments, and count times of 20–100 ms per increment depending on the relative sensitivity and the abundance of atomic species. The signal-to-noise ratios of the detailed spectra were improved by carrying out 20–100 repetitions over the region of interest.

As the aim of these experiments was to determine the valence of Ti, particular attention was paid to the Ti 2*p* envelopes. In the case of the pure tetravalent state, these consist of a doublet $2p_{3/2,1/2}$ with a splitting of 5.8 eV; the binding energy corresponding to the tetravalent $2p_{3/2}$ state is 458.7 eV in TiO_2 (Sayers and Armstrong, 1978). Furthermore, it is known that the binding energies of Ti $2p_{3/2}$ electrons in trivalent and divalent states are shifted to lower binding energies by 2.0 and 3.6 eV, respectively (Sayers and Armstrong, 1978).

There are two ways in which to proceed with the fitting of peak envelopes that have contributions from more than one valence state. First, one can in principle generate total envelopes characteristic of any mixture of Ti valence states by suitable scaling and superposition of shifted envelopes and by using known binding energies, shifts, and peak widths. In practice, however, this approach may be tedious and ambiguous as it is usually necessary to include "skewness" as well as adding Lorentzian contributions to Gaussian line shapes (Sherwood, 1983). Alternatively, when suitable standards are available, it is more straightforward to compare two experimental envelopes, one of which is characteristic of a known compound with the relevant species in a well-defined valence state. This latter method was used in the present study, in which the standard TiO_2 surface was analyzed in order to generate a Ti 2*p* envelope for tetravalent Ti–O bonding.

Depth-profiled XPS

In order to justify the assumption that hollandite fracture faces were representative of the bulk, some additional information was required. Elemental abundances in the first few monolayers of the fracture faces were determined by the following standard procedure. Areas under selected peaks were measured for all species. These areas were normalized, then divided by empirical sensitivity factors so as to yield self-consistent estimates for atomic abundances that could be compared to the bulk composition of the starting materials. Ion-beam etching (5-keV Ar^+ and current density of 0.1–1 $\mu A \cdot min/cm^2$) was then carried out to a depth of several nanometers (i.e., removal of the first few monolayers), and the XPS measurements were repeated. In this manner, it was possible to ascertain whether the surface presented by fracture was comparable to the bulk.

Determination of Ti valence ratios

A detailed scan over the Ti 2*p* envelope of the standard rutile specimen is shown in Figure 3; background and satellites have been subtracted and the data smoothed by simple polynomial fitting. Detailed scans over the same envelope were obtained for all hollandite specimens and

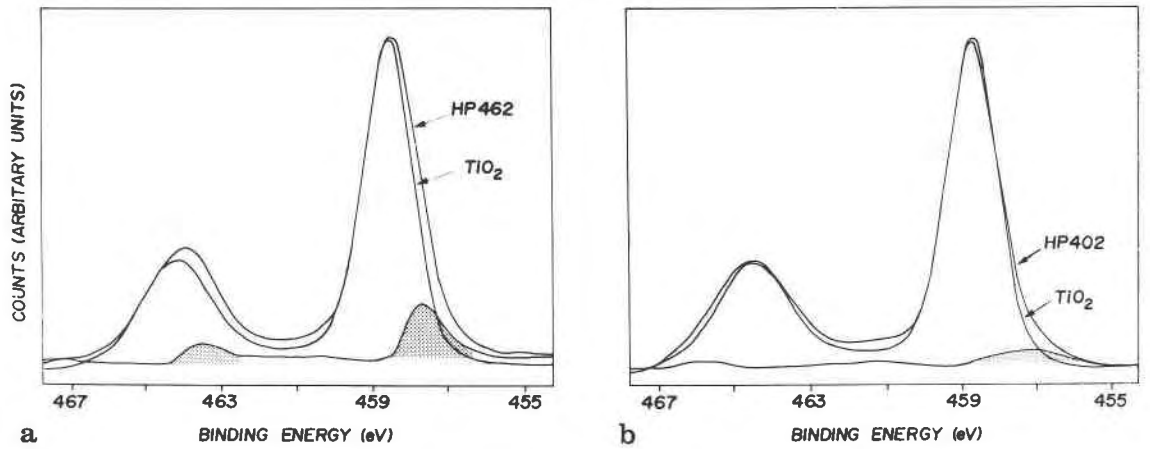

Fig. 4. Detailed scan of the Ti 2*p* envelope for specimens HP 462 (a) and HP 402 (b). Subtraction of the TiO_2 "standard" tetravalent envelope and the resultant contribution from trivalent species in the surface are shown, in stippled pattern.

subjected to similar data manipulation. Finally, all Ti 2*p* envelopes were scaled to the same arbitrary height for the $2p_{3/2}$ center maximum. The tetravalent 2*p* envelope of TiO_2 was then subtracted from the processed Ti envelopes of the hollandite samples in order to identify any trivalent Ti component. By way of example, the results of these manipulations are shown in Figure 4 for the hollandites HP 462 and HP 402 (Table 2). On the basis of microprobe data, these two hollandites were expected to exhibit the widest extremes in Ti^{3+}/Ti^{4+} ratios; the presence of Ti^{3+} in HP 462 is obvious (Fig. 4a), while for HP 402 the Ti^{3+} contribution is barely visible above background. Similar spectra having Ti^{3+} to Ti^{4+} admixtures intermediate between those presented were generated for other hollandite specimens, but for the sake of brevity are not shown. In Table 3 are summarized the Ti^{3+}/Ti^{4+} ratios as determined by EMPA and XPS for the hollandites studied. The two sets of data are in qualitative agreement; smaller Ti^{3+}/Ti^{4+} ratios are detected by both techniques for HP 402 (Ti^{3+} deficient) than for HP 462 (Ti^{3+} rich). However, the differences in absolute terms between the results are in places substantial. Significantly, the Ti^{3+}/Ti^{4+} ratios as determined by XPS are consistently smaller than the EMPA values. It is likely that this is attributable to the fact that XPS averages over a relatively large sample surface, whereas the microprobe data represent a mean of many analyses collected from individual hollandite crystallites. Therefore, XPS analyses will be affected by an additional Ti^{4+} content, present in the minor rutile phase, leading to lower than expected Ti^{3+}/Ti^{4+} ratios.

The interpretation of the results above is clearly affected by the extent to which the fracture surface is representative of the bulk composition and chemical states. For instance, it is known that fracture of hollandite-bearing polyphase titanate ceramics occurs predominantly along glassy intergranular films (usually ~1 nm wide), and that Cs may be concentrated in these films (Cooper et al., 1986). In order to determine the significance of this, hollandite fracture surfaces were ion-beam etched to an integrated dose of about 40 $\mu A \cdot min/cm^2$, which is equivalent to the removal of some 1–5 nm of surface material. [The precise etch rate is uncertain since the fracture surface is irregular, and the relationship between ion-sputtering rate and the speed of monolayer removal is not well known for titanates (Myhra et al., 1985).] The areas under the characteristic XPS peaks were monitored during the ion etching so that compositional profiles could be obtained as a function of depth. Typical data are given for HP 462 and HP 402 in Figure 5. It can be seen that Cs is enhanced in the near-surface layers (i.e., along grain-boundary films) at the expense of Ti but that the concentrations of all species approach the bulk composition of the starting material at a depth of approximately 0.5 nm. These results are summarized in Table 4. Ti valence ratios were not calculated for the etched surfaces, since ion-beam bombardment introduces electronic damage and both divalent and trivalent species are known to become more prevalent (Myhra et al., 1983). Therefore, it is generally impracticable to determine by ion-beam etching the chemical changes in speciation with depth. However, it is possible to use angle-resolved XPS measurements for nondestructive depth analysis of chemical environments in the first few monolayers.

From consideration of the data presented in Figure 5 and Table 4, it is apparent that Cs segregation is confined to a few monolayers and that in these regions, Ti abundance is no lower than 80% of the bulk value. Small changes

TABLE 3. Ti^{3+}/Ti^{4+} ratios for hollandite $[Ba_xCs_y]$-$[(Al,Ti^{3+})_{2x+y}Ti^{4+}_{8-2x-y}]O_{16}$

Specimen no.	Ti^{3+}/Ti^{4+} (%)	
	EMPA	XPS
HP 462	26	18
HP 465	18	15
HP 463	20	15
HP 410	18	10
HP 402	10	3

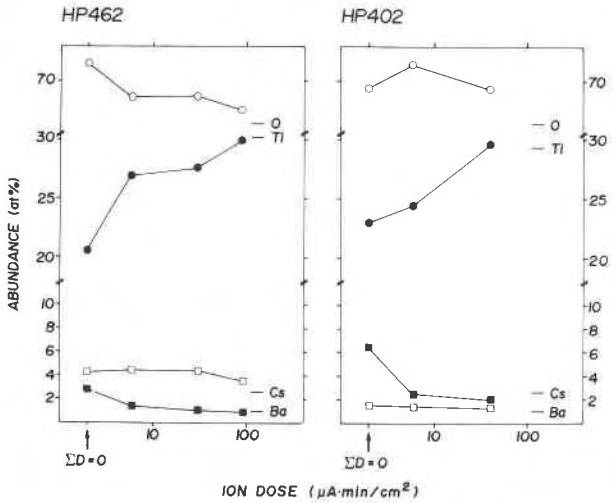

Fig. 5. Elemental abundances vs. ion etching dose (D) for HP 462 and HP 402. The nominal bulk composition is shown. $\Sigma D = 0$ data are for a fresh fracture face. O = oxygen, ● = Ti; □ = Ba, ■ = Cs.

in the characteristics of interfacial regions (Cs enhancement and layer thickness) are primarily due to different eutectic reactions between rutile and hollandite for the various compositions. Those hollandites with the highest Cs concentration have the lowest eutectic, so that during hot pressing, partial melting occurs, and the formation of wider intergranular films are favored. However, beyond this modified intergranular region, the fracture faces are representative of the bulk composition.

Conclusions

It is useful to summarize the conditions for which the procedures used in the present limited context may be exploited generally.

1. Routine XPS techniques are capable, in principle, of establishing the valence of multivalent elements when these species exhibit chemical shifts of 1 eV or more. Smaller shifts require more detailed analyses, and greater attention of the signal-to-noise ratio. For the majority of ionic species, the characteristic XPS binding energies are known and are documented in the review and/or applications literature [for collated data, see Briggs and Seah (1983)]. Although we have emphasized the application of XPS to transition-metal species, it has been successfully applied to determining the valence of rare-earth elements and U in titanate minerals (Szajman et al., 1987).

2. Formerly, the major constraint of XPS analysis was the necessity for a large (>1 mm²) representative surface to be accessible. However, recent instrument advances make it possible to do selected-area XPS under certain favorable circumstances (Riviere, 1986). Furthermore, the surface must be clean, and the chemical environment of the relevant atomic species in the first two or three monolayers must be substantially similar to that in the bulk. For a nonreactive material (i.e., one resistant to change by exposure to laboratory ambient conditions) a fractured or cleaned surface should be prepared immediately prior to insertion into the UHV chamber. If the surface is highly reactive, cleavage must be carried out in situ under extreme UHV conditions. The experimentalist should also be aware that some cleaved or fractured surfaces may undergo substantial reconstruction or be highly defective.

Table 4. Relative enhancement of Cs and depletion of Ti within intergranular films (IF) compared to the bulk composition

Specimen no.	Cs_{IF}/Cs_{bulk}	Ti_{IF}/Ti_{bulk}	Intergranular film thickness* Ion dose (μA·min/cm²)	Intergranular film thickness* Width (nm)
HP 462	3	0.8	3 ± 0.5	0.3
HP 465	3	0.8	5 ± 0.5	0.5
HP 463	4	0.8	5 ± 0.5	0.5
HP 410	2.5	0.9	1.5 ± 0.5	0.2
HP 402	3	0.9	3 ± 0.5	0.3

* Intergranular film thicknesses are estimated from the ion dose required to reach bulk composition. An average etching rate of 0.1 nm per μA·min/cm² has been assumed. The systematic uncertainty within this conversion factor may be as large as a factor of two, but it will not affect the relative accuracy.

3. Curve synthesis of "standard" spectra is feasible only in rare instances (Sherwood, 1983). In general, it is more straightforward to generate standard spectra from the analysis of compounds that are related chemically and structurally (i.e., possess the same anionic coordination number) to the "unknown" specimen. Standards must have the relevant atomic species in known valence states.

4. The XPS technique is not applicable to trace-element concentrations. Routine identification of valence states is feasible only when the atomic species is present in concentrations >1 at.%. Although most species are detectable below this level, the signal-to-noise ratio may not be sufficiently high to determine peak position and the shape of the envelope with the required accuracy.

5. Most minerals are good electrical insulators. Therefore the application of surface analytical techniques such as XPS, AES–SAM, and dynamic SIMS gives rise to charging. This is a serious problem when accurate information on binding energies is required. For XPS there are several ways of taking account of charging shifts (Swift et al., 1983). For instance, X-ray–induced Auger peaks can be measured in order to determine the so-called Auger parameter, which is independent of charging and most other experimental artifacts. Or, one may be able to deduce the charging shift and correct for it by scanning over a peak with known binding energy, i.e., by using a "marker." Another popular method is to use a flood of low-energy electrons from an auxiliary source, either to discharge the surface, or at least to stabilize the degree of charging.

Acknowledgments

The present study was undertaken with support from the Australian National Energy Research, Development and Demonstration Program. One of the authors (S.M.) is especially indebted to the Surface Analysis section at the Harwell Laboratory for the hospitality and support extended during a period of attachment.

References cited

Adams, J.M., Evans, S., Reid, P.I., Thomas, J.M., and Walters, M.J. (1977) Quantitative analysis of aluminosilicates and other solids by X-ray photoelectron spectroscopy. Analytical Chemistry, 49, 2001–2008.

Aldridge, L.P., Bill, E., Bläs, R., Lauer, S., Marathe, V.R., Sawaryn, A., Trautwein, A.X., and Winkler, H. (1986) Electronic structure of Fe in some minerals, derived from iterative extended Hückel theory (IEHT), multiple scattering Xα (MS-Xα) calculations, and Mössbauer measurements. American Mineralogist, 71, 1015–1021.

Bancroft, G.M., Brown, J.R., and Fyfe, W.S. (1979) Advances in, and applications of, X-ray photoelectron spectroscopy (ESCA) in mineralogy and geochemistry. Chemical Geology, 25, 227–243.

Bonnin, D., Calas, G., Suquet, H., and Pezerat, H. (1985) Sites occupancy of Fe^{3+} in Garfield nantronite: A spectroscopic study. Physics and Chemistry of Minerals, 12, 55–64.

Briggs, D., and Seah, M.P., Eds. (1983) Practical surface analysis by Auger and X-ray photoelectron spectroscopy. Wiley, New York.

Cooper, J.A., Cousens, D.R., Hanna, J.A., Lewis, R.A., Myhra, S., Segall, R.L., Smart, R.St.C., Turner, P.S., and White, T.J. (1986) Intergranular films and pore surfaces in Synroc C: Structure, composition and dissolution characteristics. American Ceramic Society Journal, 69, 347–352.

Dyar, M.D., and Burns, R.G. (1986) Mössbauer spectral study of ferruginous one-layer trioctahedral micas. American Mineralogist, 71, 955–965.

Evans, S., and Raftery, E. (1982) Determination of the oxidation state of manganese in lepidolite by X-ray photoelectron spectroscopy. Clay Minerals, 17, 477–481.

Herber, R.H. (1982) Mössbauer effect. In Encyclopedia of science and technology, vol. 8, p. 754–757. McGraw-Hill, New York.

Hochella, M.F., Harris, D.W., and Turner, A.M. (1986a) Scanning Auger microscopy as a high-resoluton microprobe for geologic materials. American Mineralogist, 71, 1247–1257.

Hochella, M.F., Turner, A.M., and Harris, D.W. (1986b) High resolution scanning Auger microscopy of mineral surfaces. Scanning Electron Microscopy II, 337–349, SEM Inc., AMF O'Hare, Chicago.

Hofmeister, A.M., and Rossman, G.R. (1984) Determination of Fe^{3+} and Fe^{2+} concentrations in feldspar by optical absorption and EPR spectroscopy. Physics and Chemistry of Minerals, 11, 213–224.

Kesson, S.E., and White, T.J. (1986) $[Ba_xCs_y][(Ti,Al)^{3+}_{2x+y}Ti^{4+}_{8-2x-y}]O_{16}$ synroc-type hollandites: I. Phase chemistry. Proceedings of the Royal Society (London), A-405, 73–101.

Myhra, S., Bishop, H.E., and Riviere, J.C. (1983) Investigation by XPS of surface features of some titanate minerals. Surface Technology, 19, 161–172.

Myhra, S., Savage, D., Atkinson, A., and Riviere, J.C. (1984) Surface modification of some titanate minerals subjected to hydrothermal chemical attack. American Mineralogist, 69, 902–909.

Myhra, S., Bishop, H.E., and Riviere, J.C. (1985) Features of fracture faces in Synroc C. Surface Technology, 25, 259–272.

Nefedov, V.I., Urosov, V.S., and Kakhana, M.M. (1972) X-ray photoelectron spectroscopy of bonds in Na, Mg, Al, and Si minerals. Geochemistry International, 9, 7–13.

O'Nions, R.K., and Smith, D.G.W. (1971) Investigations of the L_{II-III} X-ray emission spectra of Fe by electron microprobe. Part 2. The Fe L_{II-III} spectra of Fe and Fe-Ti oxides. American Mineralogist, 56, 1452–1463.

Otten, M.T., Miner, B., Rask, J.H., and Buseck, P.R. (1985) The determination of Ti, Mn and Fe oxidation states in minerals by electron energy loss spectroscopy. Ultramicroscopy, 18, 285–289.

Riviere, J.C. (1986) Surface analysis—Current capabilities. Zeitschrift für Analytische Chemie, 324, 728–744.

Sayers, C.N., and Armstrong, N.R. (1978) X-ray photoelectron spectroscopy of TiO_2 and other titanate electrodes and various standard titanium oxide materials: Surface compositional changes of the TiO_2 electrode during photoelectrolysis. Surface Science, 77, 301–309.

Schott, J., and Berner, R.A. (1983) X-ray photoelectron studies of the mechanism of iron silicate dissolution during weathering. Geochimica et Cosmochimica Acta, 47, 2233–2240.

Sherwood, P.M.A. (1983) Data analysis in X-ray photoelectron spectroscopy. In D. Briggs and M.P. Seah, Eds., Practical surface analysis by Auger and X-ray photoelectron spectroscopy, App. 3, p. 445–475. Wiley, New York.

Smart, R.St.C. (1985) The validity of SIMS observations of alkali metal segregation into intergranular films in ceramics. Applications of Surface Science, 22/23, 90–99.

Swift, P., Shuttleworth, D., and Seah, M.P. (1983) Appendix 2. In D. Briggs and M.P. Seah, Eds., Practical surface analysis by Auger and X-ray photoelectron spectroscopy. Wiley, New York.

Szajman, J., Smart, R.St.C., and Myhra, S. (1987) XPS studies of valence states of cerium and uranium in Synroc C. Surface and Coatings Technology, 30, 333–342.

Thames, M.T., Peterson, D.A., Hartley, J.N., and Freeman, H.D. (1981) Solving mineral processing problems with advanced surface science techniques. In D.M. Hausen and W.C. Park, Eds., Proceedings of the 110th AIME annual meeting; Process mineralogy, extractive metallurgy, mineral exploration, energy resources, p. 63–88. American Institute of Mineralogy and Metallurgy, Chicago, Illinois.

Manuscript received April 21, 1987
Manuscript accepted September 22, 1987